AIP | Applied Physics Letters

# Controllable light diffraction in woodpile photonic crystals filled with liquid crystal

Chih-Hua Ho, Yu-Chieh Cheng, Lina Maigyte, Hao Zeng, Jose Trull, Crina Cojocaru, Diederik S. Wiersma, and Kestutis Staliunas

Citation: Applied Physics Letters **106**, 021113 (2015); doi: 10.1063/1.4905695
View online: http://dx.doi.org/10.1063/1.4905695
View Table of Contents: http://scitation.aip.org/content/aip/journal/apl/106/2?ver=pdfcov
Published by the AIP Publishing

# Controllable light diffraction in woodpile photonic crystals filled with liquid crystal

Chih-Hua Ho,[1] Yu-Chieh Cheng,[2] Lina Maigyte,[2] Hao Zeng,[1] Jose Trull,[2] Crina Cojocaru,[2] Diederik S. Wiersma,[1] and Kestutis Staliunas[2,3]
[1]*European Laboratory for Non-Linear Spectroscopy (LENS), University of Florence, via Nello Carrara 1, 50019 Sesto Fiorentino, Italy*
[2]*Departament de Física i Enginyeria Nuclear, Universitat Politècnica de Catalunya, Colom 11, 08222 Terrassa, Spain*
[3]*Institucio Catalana de Reserca i Estudis Avançats (ICREA), passeig Lluis Companys 23, 08010 Barcelona, Spain*

(Received 24 November 2014; accepted 28 December 2014; published online 13 January 2015)

An approach to switching between different patterns of light beams transmitted through the woodpile photonic crystals filled with liquid crystals is proposed. The phase transition between the nematic and isotropic liquid crystal states leads to an observable variation of the spatial pattern transmitted through the photonic structure. The transmission profiles in the nematic phase also show polarization sensibility due to refractive index dependence on the field polarization. The experimental results are consistent with a numerical calculation by Finite Difference Time Domain method. © *2015 AIP Publishing LLC*. [http://dx.doi.org/10.1063/1.4905695]

Photonic crystals (PhCs), the structures with the refractive index periodically modulated on the wavelength scale, are well known due to their peculiar ***chromatic*** dispersion properties, e.g., the band-gaps in frequency domain.[1,2] More recently, it has been found that the spatial (angular) dispersion of propagating waves in PhCs is also modified, affecting the ***spatial*** propagation properties of the monochromatic light beams in such structures.[3]

The spatial propagation of light through three-dimensional (3D) PhCs, like woodpiles, is generally complicated and difficult to control. The propagation is better understood for low order propagation bands, where the spatial dispersion curves (the iso-frequency contours) are rather simple and robust to parameter fluctuations. It is known that the iso-frequency contours develop anomalous curvatures (concave segments) close to the band edges which are at the basis of anomalous diffraction/refraction and consequently of flat lensing.[4,5] Another spatial propagation peculiarity is the angular (spatial) filtering, which features in angular distribution of light transmitted through the crystal. Spatial filtering, apart from conventional arrangement of two confocal lens system with iris in focal plane, can be also achieved by more sophisticated mechanisms such as interference,[6] indefinite media,[7] resonant grating,[8] and also in propagation through PhCs.[9,10] In the general categorization of the spatial filters (high-pass, low-pass, and band-pass), the angular filtering in our study is essentially a "stop-band" (the inverse of band-pass) filter, which blocks a range of the angular components while allows the rest ones to pass.

Spatial filtering in 3D PhCs operating in lower bands has been experimentally shown only in the microwave regime,[11] also in acoustics.[12] For wavelengths in visible range ($\lambda \sim 0.5\,\mu$m), anomalous diffraction[13] and spatial filtering[14] have been realized for high order bands of PhCs, where the high density of modes results in complicated band diagram picture. The beam shaping characteristics depend very sensitively on small changes of parameters such as the average refractive index, the refractive index contrast, and the frequency.[13,14] This sensitivity, a disadvantage to the design of controllable photonic devices, can be turned into an advantage for our purposes reported in the present article: for the switching of light propagation patterns through PhCs due to infiltrated Liquid Crystals (LCs).

Some applications based on the infiltration of LCs into PhCs or into PhCs waveguides have been proposed: LC controlled optical modulators and attenuators;[15] LC controlled chromatic bandgap-shift by applying an optical or electric field;[16] LC memory effects;[17] and also fluorescence confocal polarizing microscopy.[18] Our idea and our purpose is to observe the influence of the LC infiltrated in the 3D PhCs on the angular transmission characteristics of the beams. We choose the woodpile crystals for our experiments, since the relatively long and straight channels in a woodpile result in a large birefringence of LC filled inside the channels. We note that in other configurations, for instance, for inverted diamond photonic crystals, the infiltrated LC alignment would be more complex, and the observed effects would be rather weak. Hence, we propose and experimentally demonstrate that the variation of the refractive index due to LC birefringence and to the isotropic/nematic phase transition results in notable control over the properties of the spatial filtering obtained in woodpile PhC structures.

The idea of stop-band spatial filtering, proposed and demonstrated in Refs. 9 and 11, relies on the properties of the angular bandgaps of PhC to reflect back the waves incident at particular angles (resonant with periods of the structure). Another, more convenient configuration for spatial filtering has been proposed for structures of relatively large periods, designed in regimes of gapless conditions.[10,14] In the latter case, the waves incident at particular angles are forward-deflected to the large diffraction angles. The central angle of stop band in gapless spatial filtering, in the paraxial approximation, is given by expression[14]

 

$$\sin(\alpha) = \frac{\lambda}{2d_\perp}\left(\frac{2d_\perp^2 n}{\lambda d_\parallel} - 1\right). \quad (1)$$

Here, $n$ is the average refractive index, $d_\parallel$ and $d_\perp$ are the longitudinal (along $z$ axis) and the transverse periods (along $x$ or $y$ axis, referring to the notation in Fig. 1) of the modulation, and $\lambda$ is the wavelength of the incident wave. In order to obtain an observable and controllable filtering effect, we designed and built the structures with angular stop-band at small angles $\alpha \sim 0$, which led to the particular geometry of the woodpile structure (the particular ratio of longitudinal and transverse periods). With the chosen parameters (the longitudinal period $d_\parallel = 4\,\mu$m and the transverse period $d_\perp = 0.85\,\mu$m), we expected to observe filtering at angles of a few degrees.

The geometry of the 3D woodpile and the alignment of the LCs in the nematic phase at the even (shown by green) and the odd (shown by orange) layers in channels are as schematically shown in Fig. 1. Generally, the woodpile layers can be considered as arrays of approximately straight tubes filled with LC, where the LC molecules tend to orient along the tubes, i.e., parallel to the piles in the nematic phase as illustrated in Figs. 1(c) and 1(d). The effective refractive index of LCs depends on the angle $\theta$ between the director of LC and the vector of light polarization[19]

$$n_{eff}(\theta) = \frac{n_e n_o}{\sqrt{n_e^2 \sin^2(\theta) + n_o^2 \cos^2(\theta)}}. \quad (2)$$

When the light propagates inside the woodpile, the x-polarized beam experiences the LC refractive index $n_{oddeff} = n_o$ in the tubes of odd layers ($\theta = 90°$) and $n_{eveneff} = n_e$ in the tubes of even layers ($\theta = 0°$). The y-polarized light experiences the exchanged LC refractive index (i.e., $n_{oddeff} = n_e$ and $n_{eveneff} = n_o$) in the nematic phase. While in the isotropic phase, the random orientation of the molecules results in isotropic refractive index $n_{oddeff} = n_{eveneff} = n_i = (n_e + 2n_o)/3$, which is polarization insensitive as illustrated in Figs. 1(e) and 1(f).

The woodpiles were fabricated by Direct Laser Writing (DLW) in a negative photoresist, IP-Dip (Nanoscribe GmbH).

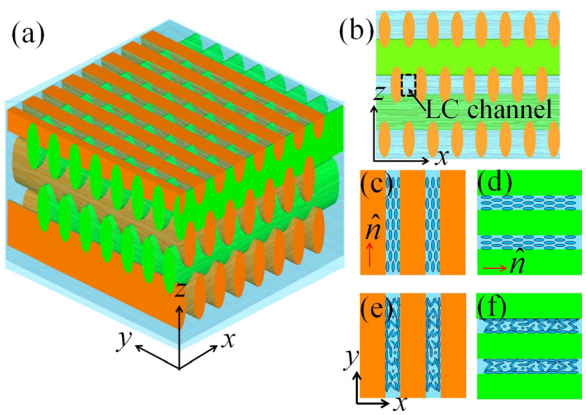


FIG. 1. (a) Schematic 3D woodpile. The insets illustrate the orientation of the directors of the LC in the channels at indicated cross sections: in $xz$ plane (b), and in $xy$ plane of the nematic phase ((c) and (d)) and of the isotropic phase ((e) and (f)). Red arrow n̂ indicates the orientation of LC director.

The tightly focused femtosecond laser beam (130 fs pulse duration, 780 nm wavelength, and 100 MHz repetition rate) focused through a 100× objective (NA 1.3) creates a solidified volume of ellipsoidal shape (0.25 $\mu$m width and 1.25 $\mu$m height with aspect ratio of 0.2) via two photon absorption polymerization. A sample translation writing speed is 100 $\mu$m/s and the laser power is 5.8 mW in front of the objective. Fig. 2 shows the Scanning Electron Microscope (SEM) images of the woodpile, which is composed of the gratings of polymer piles stacking in the longitudinal direction with four layers resulting in one period. The woodpile contains 17 periods in a total height of 68 $\mu$m; hence, it shows 11% shrinkage on the top layers. All measurements have been carried out in the central part of the woodpile, excluding the influence from defective boundary.

A micropipette is used to infiltrate the LC molecules (5CB, Sigma Aldrich) into the woodpiles with the help of a 3-axis translation stages. The strong capillary force results in complete filling of the woodpile spacing, while surface anchoring induces self-orientation of the LC molecules (Fig. 1). The multiple layers consist of alternate polymer woodpiles ($n_p = 1.54$ at 632.8 nm) and LC tubes ($n_e = 1.709$, $n_o = 1.53$, $n_i = 1.588$ at 632.8 nm), where $n_e$ and $n_o$ stand for refractive indices for the extraordinary and ordinary polarization in LC in the nematic phase and $n_i$ is the index of LC in the isotropic phase.

In experimental measurements, we focused a continuous 632.8 nm HeNe laser beam into the woodpile samples with a 50× long working distance objective and numerical aperture 0.55. The method of recording the far field transmission pattern is schematically illustrated in Fig. 3(a). A heating stage is applied to precisely control the sample temperature, in order to switch the LC component between the nematic and isotropic states. A half-wave plate was used to switch the polarization of incident beam between the $x$ and $y$ directions.

The measured far-field transmission pattern is shown in Fig. 3(b). The diffraction maxima appear at the angle of 49° corresponding to the transverse periodicity of the structure. For a quantitative characterization of the transmitted pattern, we recorded only its central part (zero diffraction maximum) by placing the screen (camera) at a distance of 30 cm behind the sample.

The numerical calculations were performed by commercial Finite Difference Time Domain (FDTD) software (CrystalWave, Photon Design). We used for the input source

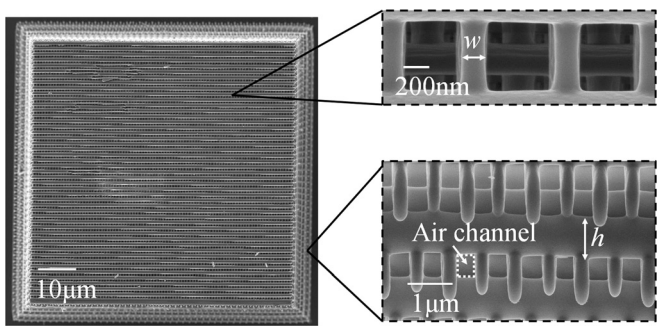


FIG. 2. SEM images of the fabricated woodpile structure before filling the air channels with LC.

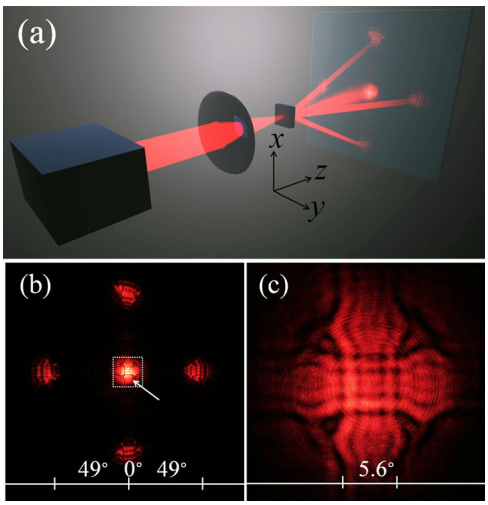


FIG. 3. Schematic experimental set-up (a), typical distribution of transmission pattern (b), and the zoom of its central part (c).

a monochromatic Gaussian beam, incident normally into the structure. A spatial stop-band filtering pattern is obtained in the far field domain of the transmitted beam for both the nematic and isotropic states. In order to simplify the 3D calculations, the 3D woodpile-LC configuration was decomposed into two separate 2D configurations.[13] This is possible if the 3D refractive index distribution $n(x,y,z)$ can be decomposed into $n(x,y,z) = n_x(x,z) + n_y(y,z)$, which approximately is the case of woodpile photonic crystals. Then, in the paraxial approximation (which does not take into account the back-reflection and assumes that the diffraction angles are not too large to the propagation direction $z$), the field can be factorized $A(x,y,z) = A_x(x,z) \cdot A_y(y,z)$. In this way, the 2D numerical calculations were performed separately for both field quadratures, highly reducing computational efforts. Specifically, the beam propagation patterns were calculated by 2D FDTD to obtain two 2D cross sections ($xz$ and $yz$ plane) as shown in Figs. 1(a) and 1(b). After Fourier transform, the far field distributions of two field quadrature directions were obtained. The full 2D cross section of the transmitted pattern in far field is then recovered by using the field factorization property.

Fig. 4 shows the measured far field spatial transmission patterns within the zero diffraction spot. The distributions show a clear presence of dark lines—deflected angular components within the central maximum, which depend on the polarization of the light and on the LC phase state. In the nematic phase (22 °C), refractive index variations of 0.01 ($n_p - n_o$) and 0.169 ($n_e - n_p$) differ strongly in each second woodpile layer. For the x-polarized beam, the angle of the horizontal filtering lines is measured to be 1.8°, and of the vertical filtering lines 5° from light beam center (Fig. 4(a)). For the y-polarized beam, the angles of horizontal and vertical filtering lines are interchanged (Fig. 4(b)). In the isotropic phase (40 °C), a low refractive index variation of 0.048 ($n_i - n_p$) shows narrower and smaller contrast filtering lines. The transmission pattern is observed for filtering angles at 1.2° and 2.8° in both directions (Fig. 4(d)). Such central symmetric pattern shows no change by rotating the polarization of incident beam.

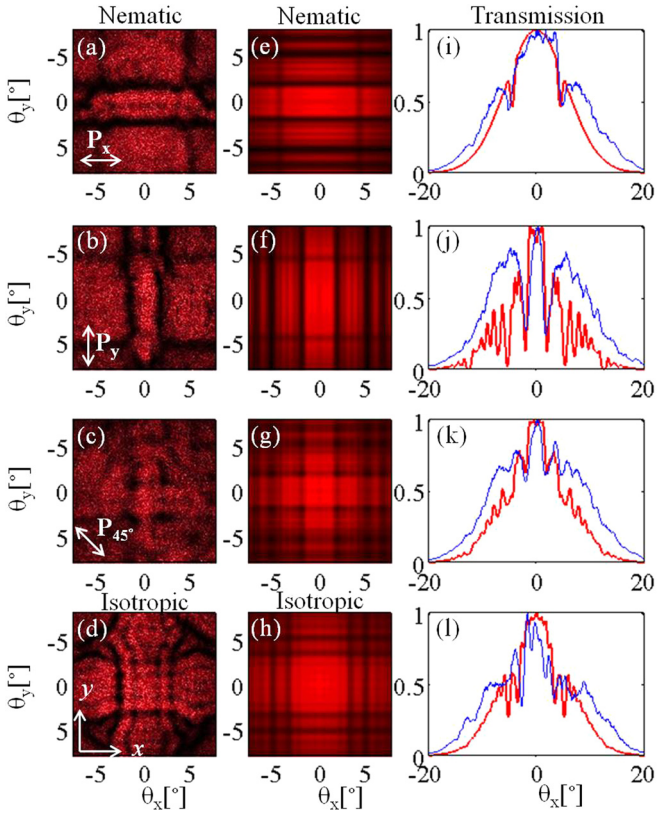


FIG. 4. 2D far field distributions of the central part beam as obtained by measurement ((a)–(d)) and FDTD calculations ((e)–(h)). The right column ((i)–(l)) compares the 1D intensity distributions along the $x$ direction (integrated along the $y$ direction) obtained from experiments (blue-solid) and from FDTD numerics (red-solid). The rows correspond to: the x-polarized beam ((a), (e), and (i)); the y-polarized beam ((b), (f), and (j)); and 45°-polarized beam ((c), (g), and (k)). The bottom row ((d), (h), and (l)) corresponds to the isotropic phase of the LC (independent on polarization).

The experimentally recorded patterns correspond well to those obtained by numerical FDTD calculations, as shown in Fig. 4. The results for the x-polarized beam (Figs. 4(a) and 4(e)) show different filtering angles in the $x$ and $y$ directions. The y-averaged 1D intensity distributions (Figs. 4(i)–4(l), along the $x$ direction) show a good agreement between the experimental results (blue), 5° in the $x$ direction (Fig. 4(i)) and 1.8° in the $y$ direction (Fig. 4(j)), and the simulated ones (red), 4.5° (Fig. 4(i)) and 2° (Fig. 4(j)), respectively. The patterns of the y-polarized beam (Figs. 4(b) and 4(f)) are simply rotated by 90° comparing to the ones for the x-polarized beam. The 45°-polarization is an average between the x- and y-polarizations. In the isotropic phase, the filtering angles are obtained at 1.2° and 2.8° in both directions, compared to two filtering lines at 3.5° and 5.2° in calculations. The angles are not sensitive to the polarization direction in latter case. The slight discrepancy between the experimental and numerical results could be due to imperfections like shrinkage, and thermal expansion of the fabricated structure. The real structure shows slightly rounded edges at the junctions of the woodpiles, which brings some discrepancy from the decomposition assumption $n(x,y,z) = n_x(x,z) + n_y(y,z)$. Further possible reason for this discrepancy is that the diffraction angles are relatively large, around 50°, which are no more in accordance with the paraxial condition.

In ***conclusion***, the spatial filtering effect of a 3D woodpile filled with embedded liquid crystal has been demonstrated. The switching effect of the spatial distribution for a light beam is measured, analyzed, and compared with the numerical study. The dependence of filtering patterns on field polarization (which induces the refractive index variation ranging from 0.01 to 0.17) appears due to the different alignments of the liquid crystal in channels at odd and even layers of the woodpile. Moreover, the phase transition between the nematic and isotropic states brings a remarkable change in spatial distribution of the propagating light beam.

Finally, we estimate the depth and width of stop-band of spatial filtering, based on analytical estimation of spatial filtering.[20] The amplitude of first harmonics of periodic index modulation (taking into account the filling factors) was estimated to be $\Delta n_0 = 0.02$. Therefore, the expected angular ranges of 0.02 rad were in accordance with the observed width of stop-band line of approximately 1°. The depth of the filtered out line, also as roughly estimated from the previous studies,[20] is $\Delta n_0 \cdot l/\lambda$ ($l$ is the length of the crystal), which for our crystal of such size was around unity, in accordance with our observations.

We acknowledge funding from Spanish Ministerio de Educación y Ciencia and European FEDER through project FIS2011-29734, from European Research Council through IIT SEED project Microswim, and from FP7/2007-2013 ERC Grant No. [291349] on photonic micro robotics. Chih-Hua Ho and Yu-Chieh Cheng are supported by the Europhotonics Erasmus Mundus Doctorate Program. We acknowledge T. Trifonov from NanoEngineering Research Center—UPC for his support with the SEM images.

[1]E. Yablonovitch, Phys. Rev. Lett. **58**, 2059 (1987).
[2]S. John, Phys. Rev. Lett. **58**, 2486 (1987).
[3]H. Kosaka, T. Kawashima, A. Tomita, M. Notomi, T. Tamamura, T. Sato, and S. Kawakami, Phys. Rev. B **58**, R10096 (1998).
[4]P. V. Parimi, W. T. Lu, P. Vodo, and S. Sridhar, Nature (London) **426**, 404 (2003).
[5]E. Cubukcu, K. Aydin, E. Ozbay, S. Foteinopoulou, and C. M. Soukoulis, Phys. Rev. Lett. **91**, 207401 (2003).
[6]L. Dettwiller and P. Chavel, J. Opt. Soc. Am. A **1**, 18 (1984).
[7]D. Schurig and D. R. Smith, Appl. Phys. Lett. **82**, 2215 (2003).
[8]A. Sentenac and A.-L. Fehrembach, J. Opt. Soc. Am. A **22**, 475 (2005).
[9]A. E. Serebryannikov, A. Y. Petrov, and E. Ozbay, Appl. Phys. Lett. **94**, 181101 (2009).
[10]K. Staliunas and V. J. Sanchez-Morcillo, Phys. Rev. A **79**, 053807 (2009).
[11]E. Colak, A. O. Cakmak, A. E. Serebryannikov, and E. Ozbay, J. Appl. Phys. **108**, 113106 (2010).
[12]R. Pico, I. Pérez-Arjona, V. J. Sánchez-Morcillo, and K. Staliunas, Appl. Acoust. **74**, 945 (2013).
[13]L. Maigyte, V. Purlys, J. Trull, M. Peckus, C. Cojocaru, D. Gailevicius, M. Malinauskas, and K. Staliunas, Opt. Lett. **38**, 2376 (2013).
[14]L. Maigyte, T. Gertus, M. Peckus, J. Trull, C. Cojocaru, V. Sirutkaitis, and K. Staliunas, Phys. Rev. A **82**, 043819 (2010).
[15]D.-P. Cai, S.-C. Nien, H.-K. Chiu, C.-C. Chen, and C.-C. Lee, Opt. Express **19**, 11890 (2011).
[16]D. McPhail, M. Straub, and M. Gu, Appl. Phys. Lett. **87**, 091117 (2005).
[17]F. Serra, S. M. Eaton, R. Cerbino, M. Buscaglia, G. Cerullo, R. Osellame, and T. Bellini, Adv. Funct. Mater. **23**, 3990–3994 (2013).
[18]H. Matthias, T. Röder, R. B. Wehrspohn, and H.-S. Kitzerow, Appl. Phys. Lett. **87**, 241105 (2005).
[19]A. Yariv and P. Yeh, *Optical Waves in Crystals: Propagation and Control of Laser Radiation* (Wiley, New York, 1984), p. 87.
[20]V. Purlys, L. Maigyte, D. Gailevičius, M. Peckus, M. Malinauskas, R. Gadonas, and K. Staliunas, Opt. Lett. **39**, 929 (2014).